A Single-Ended Fully Integrated SiGe 77/79 GHz Receiver for Automotive Radar

Li Wang, Srdjan Glisic, Johannes Borngraeber, Wolfgang Winkler, and J. Christoph Scheytt, *Member, IEEE*

***Abstract*—A single-ended 77/79 GHz monolithic microwave integrated circuit (MMIC) receiver has been developed in SiGe HBT technology for frequency-modulated continuous-wave (FMCW) automotive radars. The single-ended receiver chip consists of the first reported SiGe 77/79 GHz single-ended cascode low noise amplifier (LNA), the improved single-ended RF double-balanced down-conversion 77/79 GHz micromixer, and the modified differential Colpitts 77/79 GHz voltage controlled oscillator (VCO). The LNA presents 20/21.7 dB gain and mixer has 13.4/7 dB gain at 77/79 GHz, and the VCO oscillates from 79 to 82 GHz before it is tuned by cutting the transmission line ladder, and it centres around 77 GHz with a tuning range of 3.8 GHz for the whole ambient temperature variation range from −40 °C to +125 °C after we cut the lines by tungsten-carbide needles. Phase noise is −90 dBc/Hz@1 MHz offset. Differential output power delivered by the VCO is 5 dBm, which is an optimum level to drive the mixer. The receiver occupies 0.5 mm^2 without pads and 1.26 mm^2 with pads, and consumes 595 mW. The measurement of the whole receiver at 79 GHz shows 20–26 dB gain in the linear region with stable IF output signal. The input P_{1dB} of the receiver is −35 dBm.**

***Index Terms*—Automotive radar, flip-chip, FMCW, LNA, micromixer, MMIC, SiGe, VCO, 77/79 GHz.**

I. Introduction

AUTOMOTIVE radar products in W-band were developed in GaAs technologies decades ago because of the excellent performance of the technologies [1]–[6] etc. However, the cost of long-range radar (LRR) and short-range radar (SRR) electronics in GaAs technologies is too high to make it a commonly used security feature. Automotive radar is envisioned to save lives, e.g. in conjunction with emergency braking support in cars. In order to reduce the number of fatal accidents, considerably lower-cost solutions are needed. Additionally, the radar products should meet the ambient temperature in a wide range.

In this paper, we show a single-ended SiGe 77/79 GHz automotive radar down-conversion receiver in low-cost SiGe technology. The MMIC presented in this paper uses IHP's SiGe:C HBT self-aligned single-polysilicon BiCMOS technology with 0.25 μm minimum lithographic feature size and four/five (optional) Al metal layers [7]. Collector emitter breakdown voltage BV_{CEO} is 1.9 V. The f_T and f_{max} are up to 180 GHz and 200 GHz, respectively. The process is a low-cost high-performance process with only 25 masks and maximum reuse of CMOS process steps. The lossy substrate's resistance is 50 Ωcm.

With this technology devices and transceivers at 60 GHz [8], [9] and 77 GHz [10], [11] have been reported. The design of the integrated SiGe 79 GHz radar receiver that is described in this paper has been first presented in [11]. It builds on experience and designs from previous work, such as differential SiGe low noise amplifiers (LNAs) in common emitter topology with and without emitter degeneration at 60 GHz in [8] and [9], respectively, a single-ended cascode SiGe 77 GHz LNA with inductive degeneration [12], a single-ended cascode SiGe 77 GHz LNA without inductive degeneration [10], a differential 77 GHz SiGe Gilbert mixer [15], and an alternative 77 GHz mixer design [13] which uses the so-called "micromixer architecture" [14].

Typically a 77 GHz radar front-end uses a single-ended antenna, while the RF front-end should nevertheless yield a differential signal at its output. Due to this fact a part of the front-end will be operated with unbalanced and a part with balanced signals. There are three common types of combination of single-ended or differential LNA with single-ended or differential mixer. The first is a single-ended LNA and a single-balanced mixer. The second is a differential LNA and differential down-conversion mixer that requires an input balun. The third is using transformers/baluns between single-ended LNA and differential mixer. The mixing performance of a single-balanced mixer is worse than that of a differential mixer. The drawback of using transformers/passive baluns is larger chip area and degraded noise figure (NF) due to introduced loss. A differential LNA roughly doubles power consumption and chip area compared with a single-ended LNA. Therefore in this paper, we show a single-ended SiGe 77/79 GHz automotive radar receiver consisting of a single-ended cascode LNA, a single-ended double balanced micromixer and a differential Colpitts VCO. The comparison with the state-of-art shows excellent performance in 0.25 μm SiGe technology.

II. Circuit Design

This section discusses three major structures of radar down-conversion receiver and derives a suitable architecture consisting of a three-stage LNA, an active down-conversion micromixer, and a Colpitts VCO. These key building blocks are designed and implemented.

A. Structure of Receiver

Three different structures of receiver front-end of the radar system are depicted in Fig. 1. The LO signal and the received signals are in 77 GHz bandwidth range; the modulated output

Manuscript received December 23, 2007; revised June 27, 2007. Current version published September 10, 2008.

L. Wang is with the Department of Electronic and Electrical Engineering, University of Bristol, Bristol BS8 1UB, U.K. (e-mail: friwangli@hotmail.com).

S. Glisic, J. Borngraeber, W. Winkler, and J. C. Scheytt are with the IHP GmbH, Frankfurt (Oder) 15236, Germany.

Digital Object Identifier 10.1109/JSSC.2008.2003994

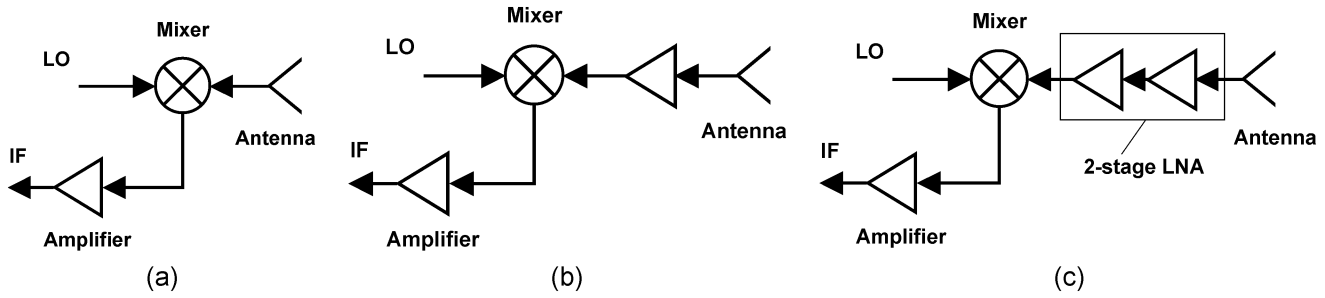

Fig. 1. Three structures of the radar receiver front-end. (a) Schottky diode down-conversion mixer. (b) With one-stage RF LNA. (c) With two-stage RF LNA.

TABLE I
SUMMARY OF TECHNICAL DATA FROM DIFFERENT STRUCTURES

Structure	Gain (dB)	Noise Figure (dB)
(a)	-8	18
(b)	7	8.5
(c)	22	7

intermediate frequency (IF) is between 50 MHz and 1 GHz. These structures are based on the commercially available GaAs MMIC.

For structure (a), a balanced Schottky diode down-conversion mixer (UMS CHM2179) is adopted. The achievable NF and conversion loss are around 18 dB and 8 dB, respectively. This structure features low NF especially at very low IF frequencies, and is the simplest structure. In structures (b) and (c), one-stage and two-stage RF LNAs are added for comparison. The RF LNA (UMS CHA 1077) shows 15 dB gain and 4.5 dB NF. Then calculating the gain and NF of the whole receiver link with Friis' formula, we get a comparison listed in Table I. From the analysis above, we could find that the additional stage of LNA in structure (b), compared with structure (a), improves the NF due to the dominance of LNA's NF in the whole link. Furthermore, additional LNA in structure (c), compared with structure (b), decreases the NF and increases the gain further.

Structure (a) realizes the simplest approach for the receiver unit. Compared to the other two structures it is advantageous in terms of packaging, since only one bare mixer die is connected to the RX-antenna. However, to achieve better NF and gain performance for receiver MMIC, we choose structure (c) consisting of a multi-stage LNA and mixer for the 77 GHz receiver front-end in our work.

The adopted radar front-end structure is shown in Fig. 2. The receiver part is marked in the dashed block. Due to limitation of the Schottky diodes mixers of this technology in W-band, we designed an active micromixer in the receiver path, and included a three-stage cascode LNA preceding it to provide gain and dominate the system NF. Therefore the noise contribution from the mixer has only little impact on the total receiver NF. Design details of the key blocks will be elaborated in the following sections.

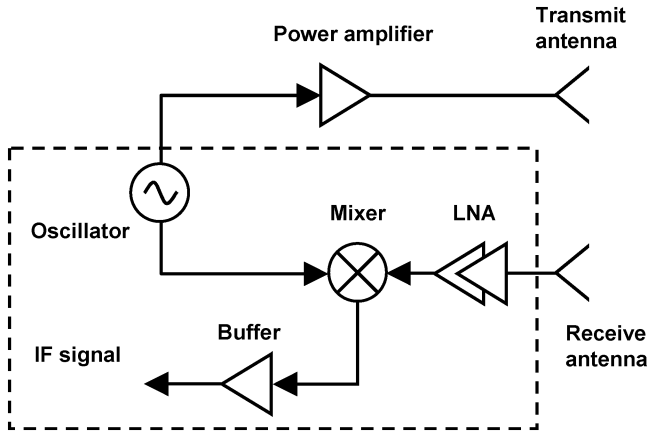

Fig. 2. Radar front-end structure adopted in this work.

B. LNA

a) Topology: There are basically three structures (shown in Fig. 3) that can be adopted in LNA design: common emitter (CE), common base (CB), and cascode structure. In the cascode configuration gain-bandwidth product is greatly improved due to elimination of the so-called Miller effect. Additionally, the cascode transistor increases the separation between the input and output ports of the cascode amplifier compared to a single CE amplifier thus improves reverse isolation. The improved isolation decreases the LO leakage to the input port of LNA and is beneficial with respect to the overall system performance. Therefore cascode structure is adopted in our design. Of course, since it includes more transistors than other structures, more noise contributors are included, so the noise figure is the slightly increased.

b) Circuit design: The single-ended LNA in cascode topology is used in a three-stage cascade [11] taking the NF, gain, and linearity into consideration, and a biasing network (Fig. 4) that provides the appropriate bias currents and voltages to the CE and CB transistors. MIM capacitors not only act as DC blockers at the input, output, and inter-stages, but also construct the matching network. Microstrip lines are used in the inductive load of each stage and the other matching networks. The probe pad is modeled as a capacitor with top metal and bottom metal as two plates in simulation.

For each stage of the LNA and the whole LNA circuit, the stability is checked and guaranteed by simulating the Mu factor and K factor. Mu factor is larger than 1 and K factor is larger than 0 for frequency ranging from 0.1 GHz to 110 GHz shown in Fig. 5(a) and (b). Additionally, the K factor is also guaranteed in temperature variation range from $-40\,^{\circ}\mathrm{C}$ to $+125\,^{\circ}\mathrm{C}$ in simulation [Fig. 5(c)].

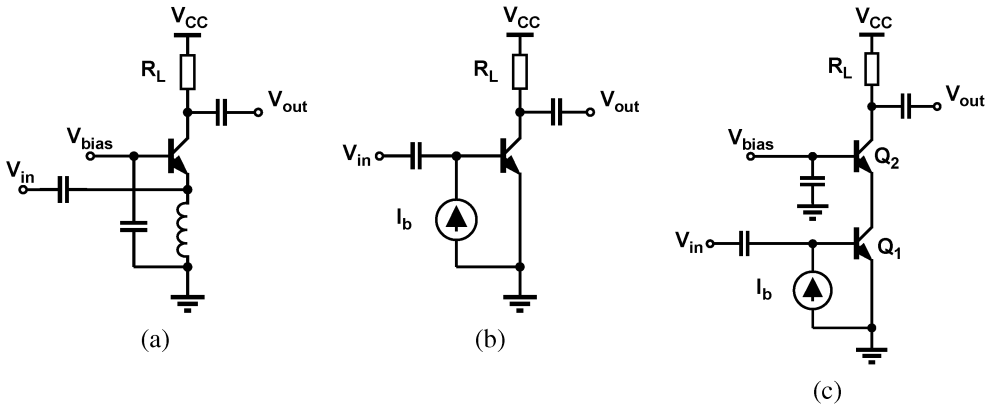

Fig. 3. Topologies of LNA circuit. (a) Common base (CB). (b) Common emitter (CE). (c) Cascode structure.

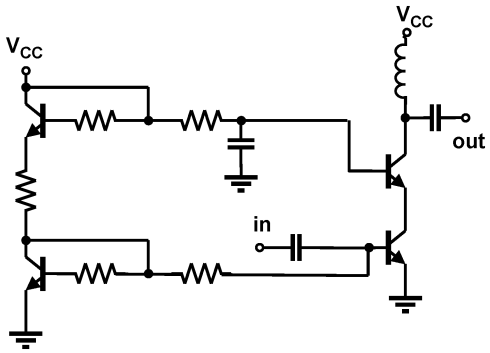

Fig. 4. One stage of three-stage cascode 77–79 GHz LNA.

The bias of the first stage is optimized to achieve minimum NF from 77 GHz to 79 GHz, and the other inter-stages are optimized to achieve maximum power gain. The optimization of the input port impedance for the first stage of LNA takes both the noise and power match into consideration, so that the minimum noise figure and maximum power transfer can be achieved simultaneously [Fig. 6(a)]. The output port is matched to impedance of the following mixer.

Fig. 6(a) shows that the input port impedance and the optimum noise source impedance are both matched to 50 Ω between 77 GHz and 79 GHz. The total NF of the LNA is matched to the $\mathrm{NF}_{\min}$ as shown in Fig. 6(b). The S-parameter simulation results will be compared with the measurement results in Section III.

C. Mixer

a) Topology: Due to the limitation of diode mixers in the available technology, we design an active mixer with gain and acceptable noise figure. Because we have designed a single-ended LNA for low power and small chip area, and we hope to avoid a transformer or balun between LNA and mixer to save chip area, therefore we adopt the single-ended RF double-balanced micromixer [14] which provides a single-ended RF port and differential LO port. We know that common base amplifier is more linear than common emitter amplifier for current amplification. Compared to the general Gilbert double-balanced mixer which feeds the RF signal to the common emitter input stage [15], the Gilbert micromixer has better linearity due to its common base RF input stage [14]. Therefore, Gilbert micromixer is preferred to have a wider linear range for the receiver. However the structures proposed in [14] have limitation for technologies with low breakdown voltages. Therefore a different structure was proposed in [13] which relaxes the limitation and improves the linearity. The 77/79 GHz micromixer in

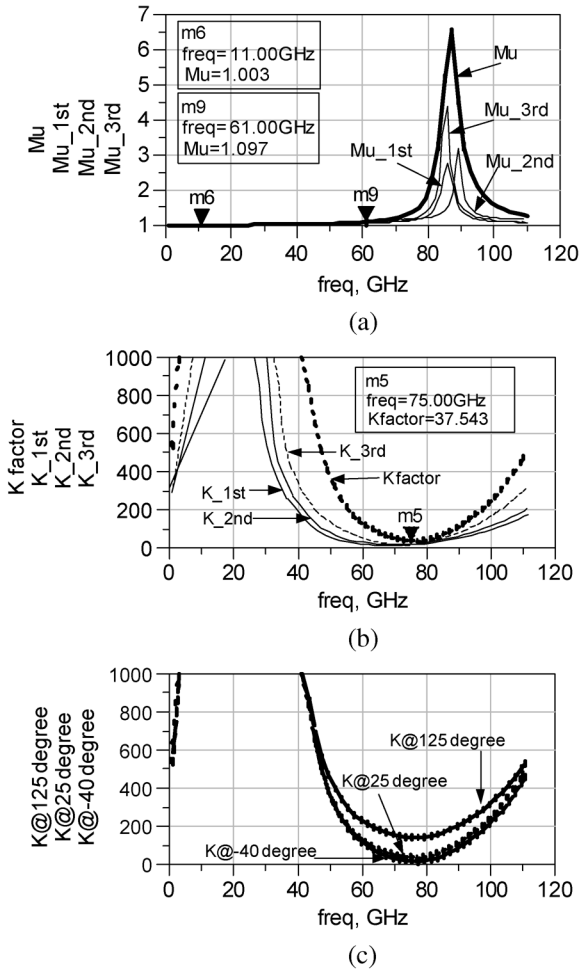

Fig. 5. Stability analysis in simulation: (a) Mu factor of each stage and the whole LNA; (b) K factor of each stage and the whole LNA; (c) K factor versus temperature.

TABLE II
COMPARISON OF PHASE AND AMPLITUDE DIFFERENCE IN ADS S-PARAMETER SIMULATION

	Type (a)	Type (b)	Type (c)	Type (new)
$(\angle(S_{21}) - \angle(S_{31}))$ °	-122.436	-106.163	-115.231	-146.606
$\lvert S_{21}\rvert - \lvert S_{31}\rvert$	0.232	0.35	0.210	0.225
S_{21} [dB] - S_{31} [dB]	5.623	11.381	4.025	5.443

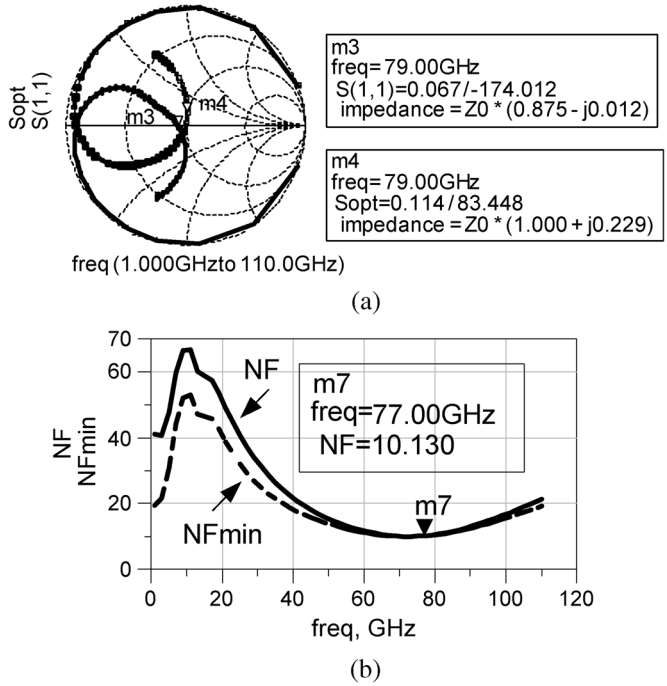

Fig. 6. (a) Optimization of input impedance for power and noise match. (b) Noise figure optimization in frequency range from 77 to 79 GHz.

the presented 77/79 GHz radar down-conversion receiver [11] uses the proposed structure.

b) Circuit design: The schematic of the whole mixer is illustrated in Fig. 7. Because the W-band source module cannot provide differential signals to the mixer quad, and if we adopt a passive transformer/balun, the output power decreases and is not enough to drive the mixer. So in order to measure the mixer's performance separately, an active LO buffer is added. This LO buffer can be removed from the receiver chip if the differential VCO can directly provide sufficient power. The LO buffer consists of a differential amplifier providing differential output signals. A 50 Ω resistor and transmission line are used at the input to provide a good match to the 50 Ω LO input port. Additionally, the LO buffer provides constant gain for the LO differential signals and provides sufficient power to drive the mixer. AC coupling is used to remove the DC offset of the differential LO signals. Furthermore, emitter followers behave as low impedance interface to the mixer core. The active LO buffer provides the function of a balun and has the advantages of smaller chip size and positive gain with little added power dissipation, compared with the disadvantages of larger chip size and loss of passive balun or transformer.

The micromixer core [13] is based on the Gilbert micromixer cell [14]. The so far reported micromixer structures are shown in Fig. 8, what differentiates our proposed structure from the existing structures is the mirrored RF branch which is marked in an ellipse circle. Q_6 is either not used or connected in different ways in the previous existing structures.

In the proposed mixer structure, Q_6 is connected in a diode form as shown in Fig. 7. The most benefit of connecting Q_6 in this way is the better balancing of the amplitude and phase of the differential RF signals. This is realized by providing a more balanced structure for RF signals at node A and B. Then this results in the cancellation of the nonlinearity of I_1 and I_3 and improves the performance of the micromixer.

To express the phase difference, we define phase for each cell in Fig. 9. Then we define the phase of the RF input signal as p_0, the phase in the left branch (at node A in Fig. 7) is p_1, and the phases in the right branch (at node B) in the existing structures (Fig. 8) and the proposed structure (Fig. 7) are p_{a2}, p_{b2}, p_{c2}, and $p_{\text{new}2}$, respectively (Fig. 10). Then the phase difference between node A and node B for each structure can be expressed by the following:

$$p_1 = p_0 + (q_{c2} - q_{e2}) \tag{1}$$

$$p_{a2} = p_0 + (q_{c1} - q_{e1}) + (q_{c2} - q_{e2}) \tag{2}$$

$$p_{c2} = p_0 + (q_{c1} - q_{e1}) \tag{3}$$

$$p_{\text{new}2} = p_0 + (q_{c1} - q_{e1}) + (q_{c3} - q_{e3}). \tag{4}$$

Then we get the phase difference between signals at node A and node B for structures (a), (c), and (new):

$$\Delta p_a = p_{a2} - p_1 = q_{c1} - q_{e1} \tag{5}$$

$$\Delta p_c = p_{c2} - p_1 = (q_{c1} - q_{e1}) - (q_{c2} - q_{e2}) \tag{6}$$

$$\Delta p_{\text{new}} = p_{\text{new}2} - p_1 = (q_{c1} - q_{e1}) + (q_{c3} - q_{e3}) - (q_{c2} - q_{e2}). \tag{7}$$

So we find that $|\Delta p_a| > |\Delta p_c|$. The ideal phase difference for two differential signals is $\pm 180°$, this means that structure (a) shows better phase balance than structure (c) for the signals at node A and node B. The equivalent circuits of the cell (1) and (3) corresponding to structure (a) and (new) are shown in Fig. 11. Connecting base and collector together in cell (3) corresponds to connecting C_{BEO} directly between emitter and collector and changing R_{BX} connection. The derivation of the equivalent impedance at node A and node B is too lengthy and it is still difficult to compare the difference. Therefore, we compare the phase and amplitude difference for four structures in ADS, and the results are listed in Table II. In three-port S-parameter simulation, port one is defined as the RF input port with phase p_0, port two is defined for phase p_1 corresponding to node A, and port three is defined for phase p_{a2}, p_{b2}, p_{c2}, and $p_{\text{new}2}$ corresponding to node B for the four structures.

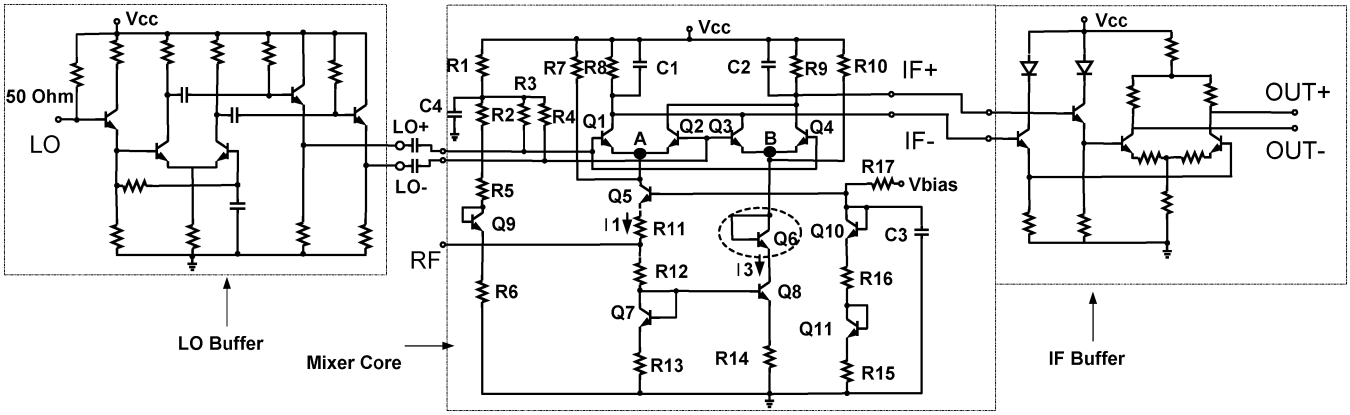

Fig. 7. Schematic of the whole mixer.

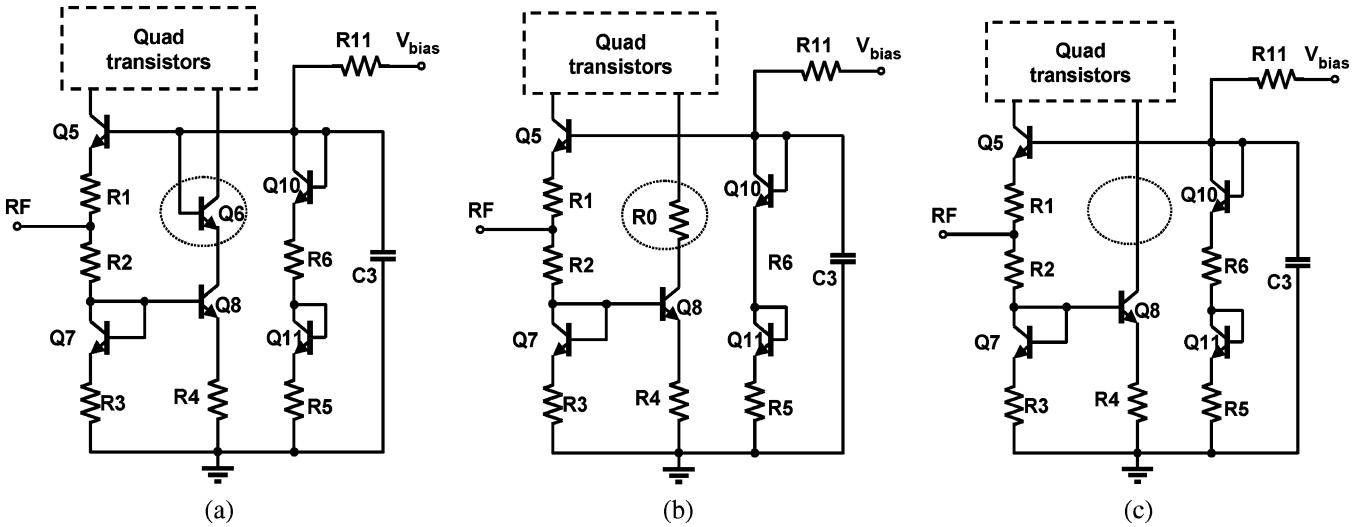

Fig. 8. Current existing micromixer structures: (a) structure in [14]; (b) structure in [18]; (c) structure in [19].

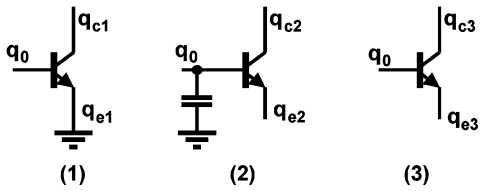

Fig. 9. Phase definitions for each cell.

In Table II we show the other four simulation results for comparison. The proposed structure shows better phase balance than the other three types because of the minimal path time delay through the junctions for RF signals at node A and B. While structure (c) has the best amplitude balance, this is because that in (c), the incidental inequality of V_{CE} of Q_8 helps to recover some current gain in the mirror lost due to its finite AC beta. Since the structure depicted in Fig. 8(c) uses no component in the mirrored RF branch, Q_8 suffers avalanche risk. This is particularly important for SiGe technologies which have low BV_{CEO}. Since BV_{CEO} is 1.9 V in f_T 180 GHz SiGe technology, V_{CE} of Q_8 is at the limit. Therefore structure (c) is not suitable for low BV_{CEO} technologies. So structure (c) will not be adopted in the design due to its risk for this technology.

To verify the improvement, three circuits are designed at 70 GHz, 77 GHz, and 84 GHz, respectively. The gain and noise figure between the proposed mixer structure and the existing micromixers are compared in simulation and illustrated in Fig. 12. We define $\mathrm{dG\_x} = \mathrm{G\_new} - \mathrm{G\_x}$, $\mathrm{dNF\_x} = \mathrm{NF\_new} - \mathrm{NF\_x}$, where G_new (or NF_new) and G_x (or NF_x) are the gain (or NF) of the new structure and structure (x) in Fig. 10, respectively; x denotes a, b, and c. The proposed structure reduces the NF compared with other three structures and the reduction is more noticeable at higher frequencies. The reason is that the individual nonlinearity of I_1 and I_3 are canceled, thus the noise interference part is removed. The improvement for the gain is also compared with structures (a) and (b) for the same reason. Compared with structure (c), the gain is reduced by 0.09 dB, 0.51 dB, and 0.15 dB at 70 GHz, 77 GHz, and 84 GHz, respectively. These results agree with the above analysis.

In summary, the proposed structure improves the linearity of the two differential RF signals and thus increases the gain, reduces the NF without increasing the complexity of the circuit and avoids the avalanche risk.

The micromixer structure provides differential RF signals to the switching quad transistors. The internal differential RF signals are achieved by the current mirror $\mathrm{Q_7}$ and $\mathrm{Q_8}$ without using

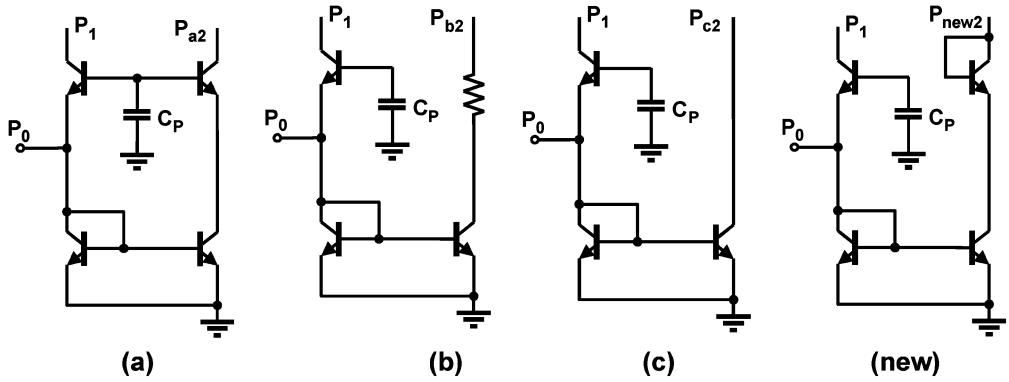

Fig. 10. Phase definitions for each structure.

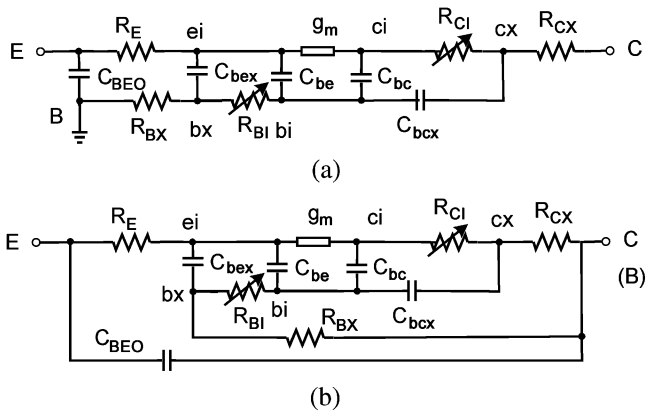

Fig. 11. (a) Equivalent circuits for cell (1). (b) Equivalent circuits for cell (3) in Fig. 9.

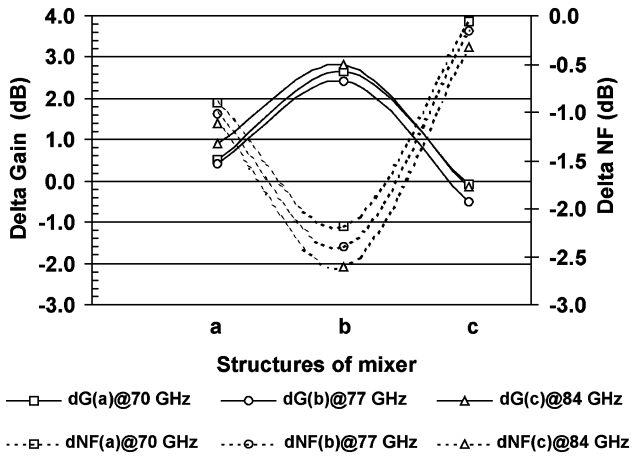

Fig. 12. Gain and NF comparison between the proposed mixer structure and the existing structures at different frequency bands.

RF balun. Thus power and chip area can be saved. Q_6 further improves the symmetry of differential RF signals [13]. The input matching for RF port is greatly facilitated by feeding the single-ended RF signal from LNA to the small resistor R_{11} that is connected to the emitter of Q_5. This linearizes the mixer further and matches the RF port to 50 Ohm or to the proceeding LNA. Additionally, tuning the control voltage V_{bias} can further finely optimize the matching. R_7 and R_{10} are used to inject current and increase the gain without increasing the tail current and power consumption [17].

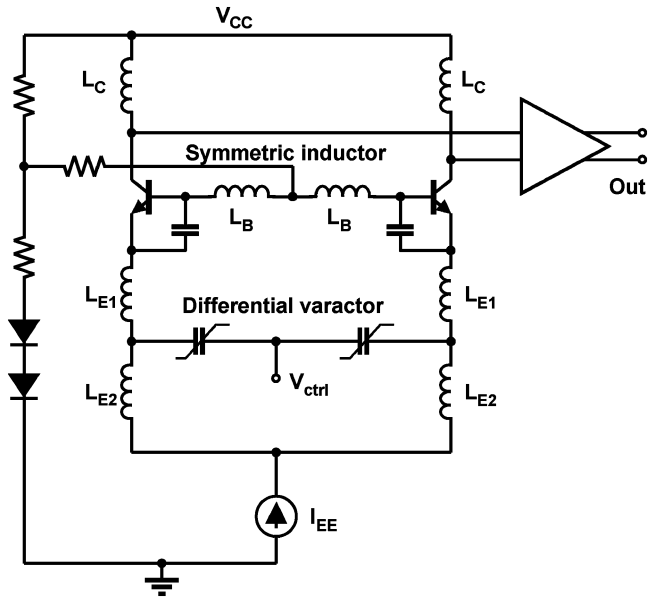

Fig. 13. Simplified schematic of VCO.

An IF output buffer is followed to match to the 50 Ω interface. To avoid the influence of IF buffer to the measurement of mixer, the gain of the IF buffer is designed to be only 1 dB in simulation. Therefore the gain and noise figure of mixer core are not influenced in measurement.

D. Voltage Controlled Oscillator (VCO)

The oscillator features a differential Colpitts topology, which has been a common choice in millimeter-range VCOs for low phase noise applications [20]–[23]. Its simplified schematic in Fig. 13 shows a modified differential Colpitts topology [20], with inductance L_{E2} in parallel, and inductance L_{E1} in series to the varactor. Adding L_{E1} and L_{E2} reduces oscillator phase noise by increasing the loaded quality factor of the resonant circuit compared to the case of a pure varactor [20].

From the Leeson formula [23] it is clear that we have to increase Q-factor of the tank and voltage swing in the tank to minimize the oscillator phase noise. In the mm-wave range Q-factor is primarily limited by the varactor.

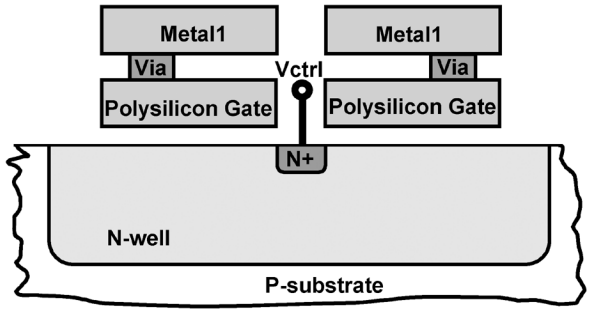

Fig. 14. Layout of varactor used in VCO.

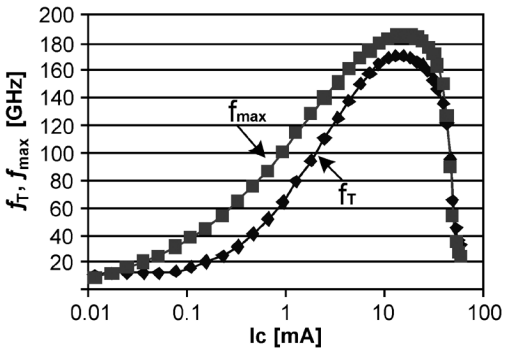

Fig. 15. Measured $f_{\mathrm{T}}/f_{\max}$ for an HBT with emitter area 1.41 $\mu\mathrm{m}^2$.

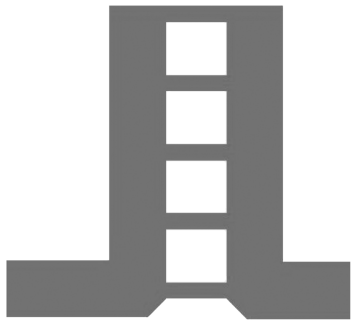

Fig. 16. Ladder structure of a line in top-metal layer.

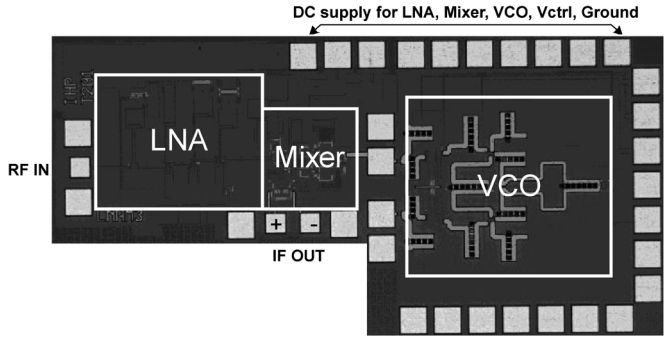

Fig. 17. Die photo of the 77/79 GHz radar receiver.

Circuits for the automotive radar applications have to operate in a large range of ambient temperature variation between $-40\,^{\circ}\mathrm{C}$ and $+125\,^{\circ}\mathrm{C}$. Capacitance of a MOS varactor is much more stable for ambient temperature change compared to an HBT varactor capacitance. This makes the MOS varactor the preferred choice for automotive radar applications.

A differential MOS varactor with lower resistance was used (see Fig. 14). It has two MOS varactors, which are connected directly in silicon. This silicon connection has small resistivity because the varactors are just 0.3 μm apart. This structure avoids contacts from N-well to Metal1 reducing varactor resistance, and hence increasing the varactor Q. There is an additional contact to the N-well (not shown in the Fig. 14) for hole extraction, which are generated for negative gate voltages.

For the VCO biasing we have to take into account maximum transistor amplification and minimum noise figure. To achieve large voltage swing in the tank we should bias VCO core transistors for the maximum transient/oscillation frequencies $f_{\mathrm{T}}/f_{\max}$. However, to minimize phase noise transistors should be biased for the minimum noise figure. As we can see in Fig. 15, $f_{\max}$ maximum of 185 GHz is reached for collector current of 15 mA, which corresponds to collector current density of 10.6 $\mathrm{mA}/\mu\mathrm{m}^2$. Noise figure of transistors can be measured only up to 30 GHz due to equipment limitation. Noise figure values in the model for higher frequencies are results of extrapolation. Simulation shows that minimum noise figure at 77 GHz is around 7 dB. For collector current of 15 mA noise figure is just fractionally higher—justifying transistor biasing for maximum f_{T} and $f_{\max}$.

Inductances, shown in the schematic, are realized in layout by transmission lines. Top metal layer, with thickness of 3 μm, is used for the signal line. It is 9 μm above the bottom metal layer, which is the ground plane. Transmission line layouts contain a ladder-type structure as can be seen in layout (Fig. 16). After chip fabrication it is possible to cut the shortening lines in this structure and effectively increase the length of the line, and by doing that increase the inductance of the line. This approach allows tuning the circuit after fabrication and avoids re-fabrication in case of detuned circuit. Shortening lines can be cut passively using tungsten-carbide needles, which are hard and sharp with tip radius of 2 μm.

VCO is followed by a single-stage buffer that features cascode topology. The single-ended power level of one to two dBm, required by the mixer, can be achieved without any buffer stage. The purpose of the buffer is to isolate the VCO core from the rest of the circuit. Cascode topology offers good isolation and matching.

VCO and buffer supply voltage is 5.5 V. This high voltage is not necessary to achieve good performance of the circuit, but it is a planned value for the supply voltage in automotive radar application [20]. Same performance could be achieved with supplied voltage less than 4 V.

III. Measurement Results

pThe 77/79 GHz radar down-conversion receiver consisted of the aforementioned three key blocks. The chip photo is shown in Fig. 17. The whole chip area is 1.26 mm^2 including pads and 0.5 mm^2 without pads. The measurement of the individual block and the whole receiver will be shown in the following sections.

A. LNA

The LNA is measured on wafer with DC $\sim$110 GHz S-parameter equipment, and is unconditionally stable in the

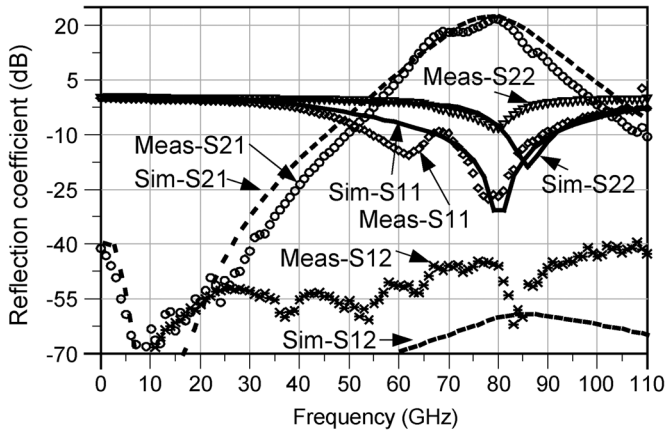

Fig. 18. Measurement and simulation results of 77–79 GHz LNA.

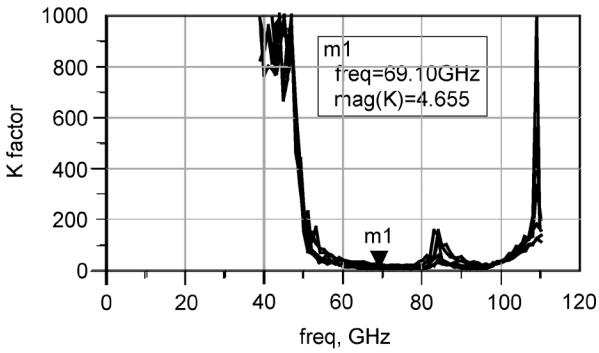

Fig. 19. Measured K factor of LNA at 27, 50, 70, 85, 100, and 125 degrees.

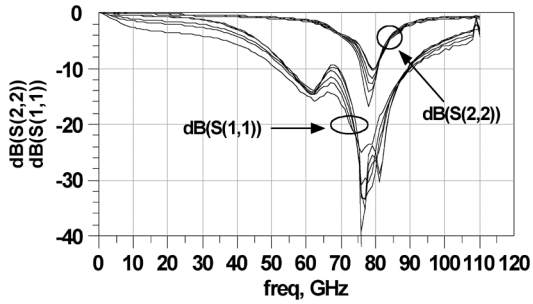

Fig. 20. Measured S(1,1) and S(2,2) of LNA at 27, 50, 70, 85, 100, and 125 degrees.

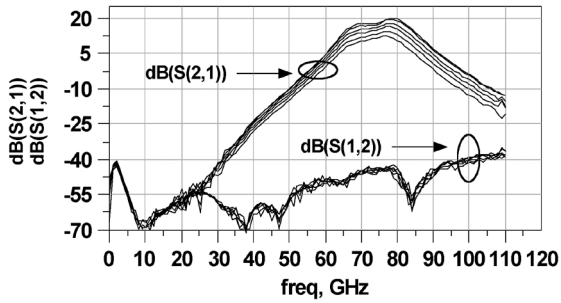

Fig. 21. Measured S(1,2) and S(2,1) of LNA at 27, 50, 70, 85, 100, and 125 degrees.

whole frequency range. The on-wafer measured S-parameter results at room temperature are shown together with the simulation results in Fig. 18, This result [11] shows improvement of in-band gain over [10], which was the first reported SiGe 77∼79 GHz single-ended cascode LNA and showed 3 dB gain ripple between 77 GHz and 79 GHz. In [11], the measured peak gain S_{21} is 21.7 dB at 79 GHz and 20 dB at 77 GHz, 1 dB gain ripple is between 77 GHz and 81 GHz, and 3 dB bandwidth is from 74 GHz to 83 GHz. S_{11} and S_{22} measurement results show that good input and output port impedance match are achieved at 77 GHz and 79 GHz. Additionally, port isolation S_{12} is larger than 45 dB in this range.

The LNA is also measured on wafer in available temperature variation range between 27 and 125 degree. The measured K factor extrapolated from the measured S-parameter versus temperature (Fig. 19) shows the unconditional stability. The LNA's gain varies from 21.7 dB@27 °C to 11.3 dB@125 °C and works stably (Figs. 20, 21). Due to the equipment limitation, the NF of the LNA could not be measured. Based on the agreement between simulation and measurement of highly accurate transistor model, passive elements, and S-parameter at 77∼79 GHz, we would estimate that the NF measurement should be very close to the simulation value of 10.2 dB.

All the measurement is done at 3.5 V with 30 mA current consumption. The input $\mathrm{P_{1dB}}$ of LNA is up to −20 dBm which is much higher than the reported result −40 dBm in [12]. The customers expect to have −20 dBm input compression point for SRR and LRR.

The overall performance of an LNA can be judged by the figure of merit (FOM) defined in [27]

$$\mathrm{FOM} = \mathrm{G_{max}} \bullet \mathrm{BW}/(\mathrm{NF_{avg}} - 1)/\mathrm{P_{diss}} \tag{8}$$

where $\mathrm{G_{max}}$ and $\mathrm{NF_{avg}}$ are the maximum gain and average noise figure, and both are in absolute values and not in dB, BW is the covered 3 dB bandwidth, and $\mathrm{P_{diss}}$ is the dissipated DC power by LNA. Because this FOM takes into account the very important parameters such as gain, bandwidth, noise figure, and power consumption, so it is adopted in the comparison to the measurement results of state-of-art.

Table III summarizes the recently reported 77 GHz LNAs. Our LNA shows better FOM than some in GaAs technology, and shows comparable FOM compared with others in more advanced SiGe technology.

B. Mixer

The mixer chip occupies 0.5 mm × 0.55 mm including pads, and 0.3 mm × 0.2 mm without pads. RF and LO are fed from the opposite sides to improve the isolation in layout. The separate measurement of the mixer at 77/79 GHz shows 13.4/7 dB gain (Fig. 22) and 18.4/18.72 dB NF. The receiver's compression point is dependent on both LNA and mixer. The mixer's input compression point is −12 dBm and shows better linearity than −20 dBm of the aforementioned LNA. So the compression point of the receiver is mainly limited by the LNA. The detail measurement results are included in Table IV and [13]. All the measurements were done on wafer with mm-wave source module HP 83558A and multiplier for W-band. The exact input power of LO and RF is measured by Agilent W8486A W-band power sensor and HP E4419B power meter. The NF was measured by using the W-band noise source and Aeroflex PN9000

TABLE III
COMPARISON OF FOM OF 77 GHz/79 GHz LNAs

	Vcc (V)	Current (mA)	Gain_max (dB)	NF (dB)	BW (GHz)	Technology-f_T/f_{max} (GHz)	Chip Size (mm^2)	FOM [27]
[24]	3	30	10	4	8	0.15 *um GaAs*-80/*n.a*	1.34 × 1.0	0.58
[25]	2	19.2	15	3.5	10	0.19 *um GaAs- n.a/n.a*	1.88 × 1.20	6.65
[26]	3.5	25	23.8	8	6	0.12*um SiGe*-207/285	0.86 × 0.36	2.21
[29]	5.5	32	16	6.5	4	0.18 *um SiGe*-200/275	n.a	0.164
[31]	5.5	10	26	6.0	5	0.13 *um SiGe*- n.a	n.a	7.23
[34]	3.5	17.5	23.8	6	6	0.13 *um SiGe*-200/330	n.a	4.69
[35]	5.5	22	8.9	4.8	10	0.14 *um SiGe*-225	0.45 × 0.45	0.168
This work [11]	3.5	30	21.7	10.1	9	0.25 *um SiGe*-180/200	0.42 × 0.42	1.38

TABLE IV
COMPARISON OF FOM OF 77 GHz/79 GHz MIXERS

	[29]	[38]	[15]	[31]	[36]	This work [11]
Type of Mixer	Subharmonic	Subharmonic	Gilbert	Gilbert	Gilbert	Micromixer
Vcc (V)	5	n/a	-5	67mW	n/a	4.5
Current (mA)	4.4	n/a	60		n/a	39
Conversion Gain (dB)	0.7	-14~-18	2 2	20-26	11.5	13.4
LO Power (dBm)	10	5	2	-2	0	2
LO Frequency (GHz)	38	36	77	75	77	77
SSB Noise Figure (dB)	23(sim.)	n/a	14	12-14	15.8	18.4
P_{1dB} input/output (dBm)	-8/-7.3	0	-30/-4	-26	-0.3	-12/1.3
Isolation (dB)	>30(LO-RF)	40(LO-IF)	n/a	n/a	n/a	>34(LO-RF) >28(LO-IF)
Technology (SiGe)	0.5 *um*	0.15 *um*	0.18 *um*	0.13 *um*	0.14 *um*	0.25 *um*
f_T (*GHz*)	80	n/a	200	n/a	225	180
Chip Size (mm^2)	0.86 × 0.9	1.5 × 1.0	0.55 × 0.45	n/a	0.9 × 0.7	0.5 × 0.55
FOM [28]	-99.72	n/a	-93.58	-79.26	n/a	-89.07

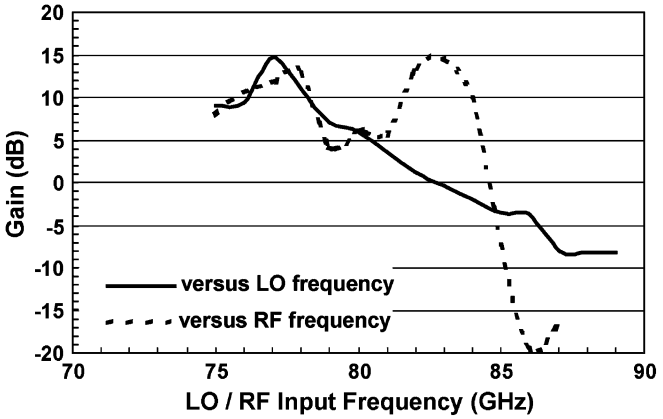

Fig. 22. Measured conversion gain of mixer versus RF and LO input frequency.

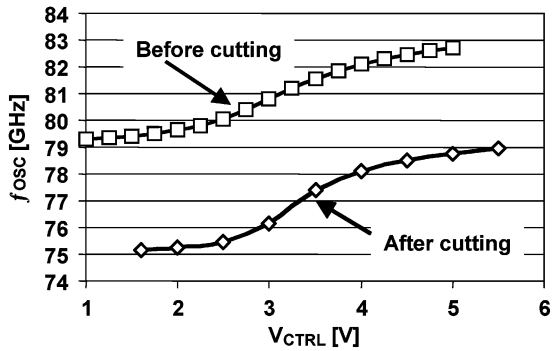

Fig. 23. Measured VCO oscillation frequency versus control voltage before/after cutting the lines.

Phase Noise Test System. To compare the performance of our mixer with the other state-of-the-art, we adopt the definition of FOM in [28]:

$$\mathrm{FOM_{MIX}} = (\mathrm{CG} - \mathrm{NF}) + (\mathrm{MIX_{LIN}} - \mathrm{NF}) - \mathrm{MIX_{PWR}} - \mathrm{MIX_{ISO}}. \quad (9)$$

The definition of each item can be found in [28]. Table IV includes the technical data of 77 GHz mixers and illustrates a comparison to the state-of-art. Since not all papers provide the isolation data, so $\mathrm{MIX_{ISO}}$ is omitted in $\mathrm{FOM_{MIX}}$. Our mixer achieves the highest $\mathrm{FOM_{MIX}}$, showing 60% better linearity with 41% less power consumption, and better $\mathrm{P_{1dB}}$ than -30 dBm compared to the reported active SiGe mixer in [15].

C. VCO

The VCO was measured on-wafer using Rohde&Schwarz spectrum analyzer FSEM30 (up to 26.5 GHz) and harmonic mixer for E-band (60~90 GHz). VCO draws 80 mA from 5.5 V supply. As shown in Fig. 23 frequency range is 3.8 GHz. Two lines in base inductance were cut to centre the frequency range around 77 GHz. Phase noise plot show in Fig. 24 was obtained

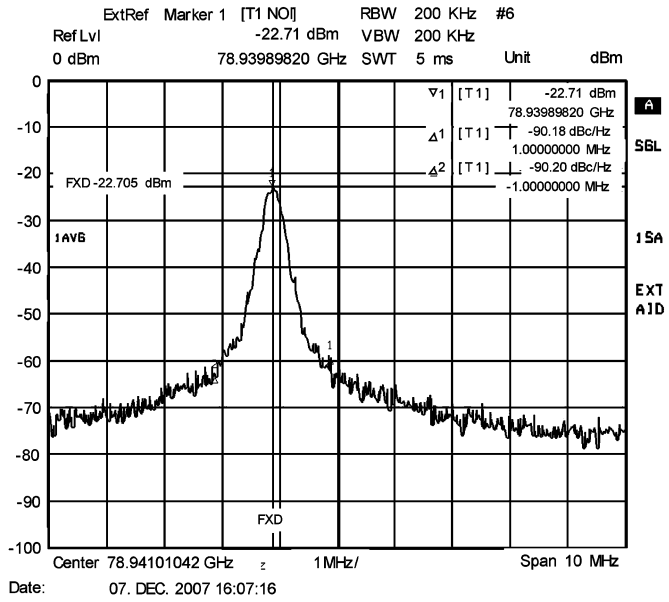

Fig. 24. Measured VCO phase noise.

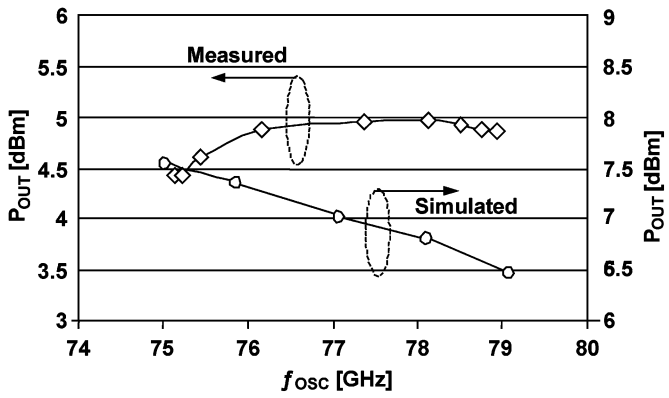

Fig. 25. Measured and simulated VCO output power as a function of oscillation frequency.

with averaging over ten sweeps for better reliability. Measured phase noise at 1 MHz offset is below -90 dBc/Hz.

Output power measurement with harmonic mixer and spectrum analyzer has unacceptably low accuracy with measurement error up to several dBs. Precise power measurements were done with a Hewlett-Packard E4419B power meter and an Agilent W8486A power sensor for W-band (75∼110 GHz). Measured differential output power is 5 dBm (Fig. 25), which is optimal level to drive the mixer. Power level is almost flat with ripple of just 0.5 dB in the whole frequency range and 0.2 dB in the frequency range of interest (76–77 GHz).

Temperature stability of oscillation frequency is shown in the Fig. 26. In the temperature range up to 125 °C we get an oscillation frequency shift $\Delta f_{\rm osc} = -1.35$ GHz/100 K. With measured frequency range of 3.8 GHz oscillating frequency is stable enough to ensure that the VCO always covers the required frequency range from 76 to 77 GHz when the ambient temperature changes from -40 °C to $+125$ °C.

The size of the VCO chip is 0.8 mm^2 with pads and 0.4 mm^2 without pads. The upper and lower raw of DC pads (see Fig. 17)

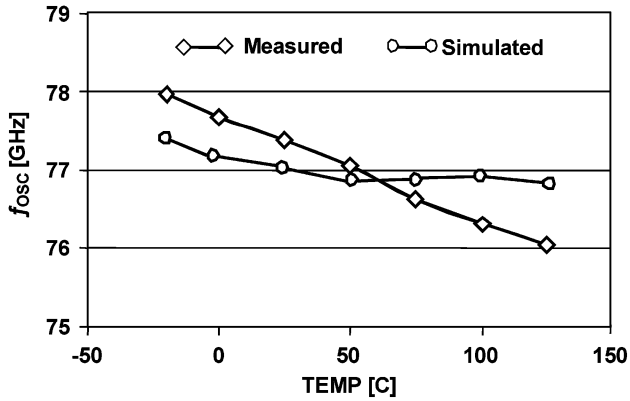

Fig. 26. VCO oscillation frequency as a function of ambient temperature in simulation and measurement.

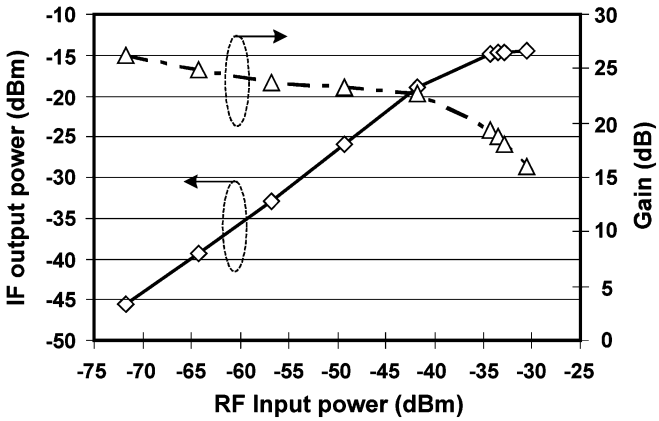

Fig. 27. Linearity and gain on-wafer measurement of the receiver.

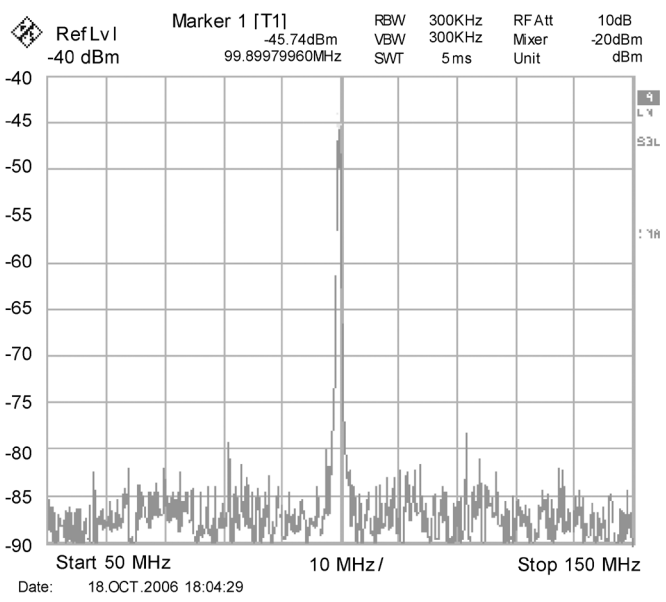

Fig. 28. IF output spectrum of on-wafer measurement of the whole radar receiver.

can be omitted because they are connected to the same control and supply voltages as pads to the right. They were put in the layout for measurement convenience.

TABLE V
COMPARISON OF 77 GHz/79 GHz RECEIVERS

	P_{dc} (mW)	Gain (dB)	NF (dB)	P_{1dB} (dBm)	SiGe Technology-f_T /f_{max} (GHz)	Chip Size (mm^2)	Notes
[29]	1072	28	11	-16	0.18 *um*-200/275	1 × 1.1	I/Q RX (LNAs, couplers, mixers)
[30]	440	30	11.5	-26	0.18 *um*-225/330	1.03 × 1.13	RX (LNA, baluns, mixer)
[31]	195	40-46	6.0 (sim.)	-38~-44	0.13 *um*- n.a	1.7 × 1	Diff. RX (LNA, mixer, VCO)
[32]	n.a	30	7	-22	0.18 *um*-195/290	3.3 × 1.3	RX (LNA, balun, mixer, buffer, doubler, etc)
[33]	740	25.6	9	-24	0.13 *um*-170/200	n.a	TX/RX (LNA, mixer, PA VCO, divider, etc)
[34]	n.a	37	8	n.a	0.18 *um*-225/330	9	RX (LNA, synthesizer, phase rotators, antennas, etc)
This work [11]	595	21.7	10.2 (sim.)	-35	0.25*um*-180/200	1.26	Single-ended RX (LNA, mixer, VCO)

D. Receiver

The on-wafer measurement of the whole receiver is performed at 79 GHz. The IF output spectrum is shown in Fig. 27. Gain at 100 MHz IF frequency is 20–26 dB after calibration (Fig. 28), which is close to the gain sum of LNA and mixer. The input P_{1dB} compression point of the whole receiver is around -35 dBm. Due to the equipment limitation when we measured the receiver, the whole NF was not measured. Because the noise contribution from mixer has been greatly reduced by the high gain of LNA, and based on the agreement of the simulation and measurement of the three separate circuits, we would estimate that the measured NF should be very close to the extrapolated value of 10.2 dB. This is lower than the required NF of 16 dB [39]. The technical data of the receiver is compared with the other state-of-the-art in Table V.

IV. CONCLUSION

This paper reports a fully integrated single-ended 77/79 GHz automotive radar down-conversion receiver that consists of a single-ended cascode LNA, a single-ended micromixer, and a differential Colpitts VCO in SiGe technology. The LNA achieves 20 dB and 21.7 dB gain at 77 GHz and 79 GHz, respectively. The micromixer works at 77 GHz and 79 GHz with 13.4 dB and 7 dB gain, and VCO provides 5 dBm sufficient power to drive the mixer while achieving a phase noise of better than -90 dBc/Hz at 1 MHz offset. The whole receiver shows 20–26 dB gain at 100 MHz IF frequency. The estimated NF of the whole receiver is 10.2 dB. Competitive performance with low power consumption, small chip area and high integration level is achieved.

ACKNOWLEDGMENT

The authors thank the IHP staff for excellent fabrication of the chips.

REFERENCES

[1] K. W. Chang, G. S. Dow, H. Wang, T. H. Chen, K. Tan, B. Allen, and J. Berrenz, "A W-band single-chip transceiver for FMCW radar," in *Proc. IEEE Microwave and Millimeter-Wave Monolithic Circuits Symp.*, 1993, pp. 41–44.

[2] A. Klaassen and J.-M. Dieudonne, "77 GHz monolithic MMIC schottkyand PIN-diode switches based on GaAs MESFET and SiGe SIMMWIC technology," in *Proc. IEEE MTT-S Int. Microwave Symp. (IMS)*, Jun. 1995, pp. 1631–1634.

[3] H. Kondoh, K. Sikine, S. Takatani, K. Takano, H. Kuroda, and R. Dabkowski, "77 GHz fully-MMIC automotive forward-looking radar," in *Proc. IEEE Gallium Arsenide Integrated Circuits (GaAs IC) Symp.*, Oct. 17–20, 1999, pp. 211–214.

[4] I. Gresham, N. Jain, T. Budka, A. Alexanian, N. Kinayman, B. Ziegner, S. Brown, and P. Staecker, "A compact manufacturable 76–77 GHz radar module for commercial ACC applications," *IEEE Trans. Microw. Theory Tech.*, vol. 49, no. 1, pp. 44–58, Jan. 2001.

[5] A. Tessmann, S. Kudszus, T. Feltgen, M. Riessle, C. Sklarczyk, and W. H. Haydl, "Compact single-chip W-band FMCW radar modules for commercial high-resolution sensor applications," *IEEE Trans. Microw. Theory Tech.*, vol. 50, no. 12, pp. 2995–3001, Dec. 2002.

[6] W. Mayer, M. Meilchen, W. Grabherr, P. Nuchter, and R. Guhl, "Eightchannel 77 GHz front-end module with high-performance synthesized signal generator for FM-CW sensor applications," *IEEE Trans. Microw. Theory Tech.*, vol. 52, no. 3, pp. 993–1000, Mar. 2004.

[7] B. Heinemann *et al.*, "Novel collector design for high-speed SiGe:C HBTs," in *IEEE IEDM Tech. Dig.*, 2002, pp. 775–778.

[8] W. Winkler, J. Borngräber, H. Gustat, and F. Korndörfer, "60 GHz transceiver circuits in SiGe:C BiCMOS technology," in *Proc. European Solid State Circuits Conf. (ESSCIRC)*, 2004, pp. 83–86.

[9] Y. M. Sun, J. Borngräber, F. Herzel, and W. Winkler, "A fully integrated 60 GHz LNA in SiGe:C BiCMOS technology," in *Proc. IEEE Bipolar/BiCMOS Circuits and Technology Meeting*, 2005, pp. 14–17.

[10] L. Wang, J. Borngraeber, and W. Winkler, "77 GHz automotive radar receiver front-end in SiGe:C BiCMOS technology," in *Proc. European Solid-State Circuits Conf. (ESSCIRC)*, Montreux, Switzerland, Sep. 2006, pp. 388–391.

[11] L. Wang, S. Glisic, J. Borngraeber, W. Winkler, and C. Scheytt, "A single-ended 79 GHz radar receiver in SiGe technology," in *Proc. IEEE Bipolar/BiCMOS Circuits and Technology Meeting*, Oct. 2007, pp. 218–221.

[12] R. Reuter and Y. Yin, "A 77 GHz (W-band) SiGe LNA with a 6.2 dB noise figure and gain adjustable to 33 dB," in *Proc. IEEE Bipolar/BiCMOS Circuits and Technology Meeting*, Oct. 2006, 7.2, 4 pp.

[13] L. Wang, R. Kraemer, and J. Borngraeber, "An improved highly-linear low-power down-conversion micromixer for 77 GHz automotive radar in SiGe technology," in *IEEE MTT-S Int. Microwave Symp. (IMS)*, San Francisco, CA, Jun. 2006, pp. 1834–1837.

[14] B. Gilbert, "The MICROMIXER: A highly linear variant of the Gilbert mixer using a bisymmetric class-AB input stage," *IEEE J. Solid-State Circuits*, vol. 32, no. 9, pp. 1412–1423, Sep. 1997.

[15] W. Perndl, H. Knapp, M. Wurzer, and K. Aufinger *et al.*, "A low-noise and high gain double-balanced mixer for 77 GHz automotive radar front-ends in SiGe:C HBT technology," in *Proc. IEEE Radio Frequency Circuits Symp.*, 2004, pp. 47–50.

[16] M. Camiade, "Overview on GaAs MMICs for automotive radar," in *24th Annu. Tech. Dig. Gallium Arsenide Integrated Circuit (GaAs IC) Symp.*, 2002, pp. 29–32.

[17] B. Razavi, *RF Microelectronics*. New York: Prentice-Hall, 1998, ch. 6.

[18] C. Meng, T.-H. Wu, T.-H. Wu, and G.-W. Huang, "A 5.2 GHz 16 dB CMFB Gilbert downconversion mixer using 0.35 μm deep trench isolation SiGe BiMCOS technology," in *IEEE MTT-S Int. Microwave Symp.*, 2003, pp. 975–978.

[19] C. Y. Wang, S. S. Lu, C. C. Meng, and Y. S. Lin, "A SiGe micromixer for 2.4/5.2/5.7 GHz multiband WLAN applications," *IEEE Microw. Opt. Technol. Lett.*, vol. 41, no. 5, pp. 343–346, Jun. 2004.
[20] H. Li and H. M. Rein, "A millimeter wave VCO with wide tuning range and low phase noise, fully integrated in a SiGe bipolar production technology," in *IEEE ISSCC Dig. Tech. Papers*, 2003, pp. 184–191.
[21] H. Li, H. M. Rein, T. Suttorp, and J. Böck, "Fully integrated SiGe VCOs with powerful output buffer for 77 GHz automotive radar systems and applications around 100 GHz," *IEEE J. Solid-State Circuits*, vol. 39, no. 10, pp. 1650–1658, Oct. 2004.
[22] S. T. Nicolson, K. Yau, P. Chevalier, A. Chantre, B. Sautreuil, K. Tang, and S. Voinigescu, "Design and scaling of W-band SiGe BiCMOS VCOs," *IEEE J. Solid-State Circuits*, vol. 42, no. 9, pp. 1821–1833, Sep. 2007.
[23] J.-C. Nallatamby and M. Prigent, "Phase noise in oscillators—Leeson formula revisited," *IEEE Trans. Microw. Theory Tech.*, vol. 51, no. 4, pp. 1386–1394, Apr. 2003.
[24] R. Eye and D. Allen, "77 GHz low noise amplifier for automotive radar applications," in *IEEE GaAs Dig.*, 2003, pp. 139–142.
[25] N. Tanahashi, K. Kanaya, T. Matsuzuka, and T. Katoh *et al.*, "A W-band ultra low noise amplifier MMIC using GaAs pHEMT," in *IEEE MTT-S Int. Microwave Symp. Dig.*, 2003, pp. 2225–2228.
[26] A. Babakhani, X. Guan, A. Komijani, A. Natarajan, and A. Hajimiri, "A 77 GHz 4-element phased array receiver with on-chip dipole antennas in silicon," in *IEEE ISSCC Dig.*, 2006, pp. 180–181.
[27] F. Ellinger, D. Barras, M. Schmatz, and H. Jankel, "A low-power DC-7.8 GHz BiCMOS LNA for UWB and optical communications," in *IEEE MTT-S Int. Microwave Symp. (IMS)*, 2004, pp. 13–16.
[28] J. P. Comeau, J. D. Cressler, J. Lee, and A. J. Joseph, "An 8.4–12.0 GHz down-conversion mixer implemented in SiGe HBT technology," in *Proc. IEEE Topical Meeting on Silicon Monolithic Integrated Circuits in RF Systems*, 2004, pp. 13–16.
[29] B. Dehlink, J.-D. Wohlmuth, K. Aufinger, F. Weiss, and A. L. Scholtz, "An 80 GHz SiGe quadrature receiver frontend," in *Proc. IEEE CSICS*, Nov. 2006, pp. 197–200.
[30] M. Hartmann, C. Wagner, K. Seemann, J. Platz, H. Jager, and R. Weigel, "A low-power low-noise single-chip receiver front-end for automotive radar at 77 GHz in silicon-germanium bipolar technology," in *IEEE MTT-S Int. Microwave Symp. (IMS)*, Jun. 2007, pp. 149–152.
[31] J. Powell, H. Kim, and C. G. Sodini, "A 77 GHz receiver front end for passive imaging," in *Proc. IEEE RFIC Symp.*, Jun. 2007, pp. 145–148.
[32] R. Reuter, H. Li, I. To, Y. Yin, A. Ghazinour, D. Jahn, D. Morgan, J. Feige, P. Welsh, S. Braithwaite, B. Knappenberger, D. Scheitlin, J. John, M. Huang, P. Wennekers, M. Tutt, C. Trigas, and J. Kirchgessner, "Fully integrated SiGe-BiCMOS Receiver (RX) and Transmitter (TX) chips for 76.5 GHz FMCW automotive radar systems including demonstrator board design," in *Proc. IEEE MTT-S Int. Microwave Symp. (IMS)*, 2007, pp. 1307–1310.
[33] S. T. Nicolson, P. Chevalier, A. Chantre, B. Sautreuil, and S. P. Voinigescu, "A 77–79 GHz Doppler radar transceiver in silicon," in *Proc. IEEE CSICS*, Oct. 2007, pp. 252–255.
[34] A. Babakhani, X. Guan, A. Komijani, A. Natarajan, and A. Hajimiri, "A 77 GHz phased-array transceiver with on-chip antennas in silicon: Receiver and antennas," *IEEE J. Solid-State Circuits*, vol. 41, no. 12, pp. 2795–2806, Dec. 2006.
[35] B. Dehlink, H.-D. Wohlmuth, K. Aufinger, T. F. Meister, J. Bäock, and A. L. Scholtz, "A low-noise amplifier at 77 GHz in SiGe:C bipolar technology," in *CSIC Dig.*, 2005, pp. 287–290.
[36] H. Knapp, B. Dehlink, H.-P. Forstner, E. Kolmhofer, K. Aufinger, J. Bock, and T. F. Meister, "SiGe circuits for automotive radar," in *Proc. 2007 Topical Meeting on Silicon Monolithic Integrated Circuits in RF Systems*, Jan. 10–12, 2007, pp. 231–236.
[37] M. F. Lei, P. S. Wu, T. W. Huang, and H. Wang, "Design and analysis of a miniature W-Band MMIC sub-harmonically pumped resistive mixer," in *Proc. IEEE MTT-S Int. Microwave Symp. (IMS)*, Jun. 2004, pp. 235–238.
[38] J.-J. Hung, T. M. Hancock, and G. M. Rebeiz, "A 77 GHz SiGe subharmonic balanced mixer," *IEEE J. Solid-State Circuits*, vol. 40, no. 11, pp. 2167–2173, Nov. 2005.
[39] W. Mayer, M. Meilchen, W. Grabherr, P. Nuchter, and R. Guhl, "Eight-channel 77 GHz front-end module with high-performance synthesized signal generator for FM-CW sensor applications," *IEEE Trans. Microwave Theory Tech.*, vol. 52, no. 3, pp. 993–1000, Mar. 2004.

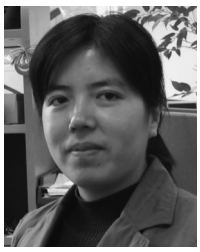

Li Wang received the Master degree in communications technology from the University of Ulm, Ulm, Germany, in 2003. In 2004, she joined the Circuit Design Department of IHP, Frankfurt (Oder), Germany, as a Ph.D. candidate. Her work was focused on the high-speed frequency dividers, millimeter-wave circuits including LNA, mixer, amplifiers, front-end system integration in 77 GHz range for automotive radar application and frequencies beyond.

Since 2006, she has worked as a Research Associate in the Electrical and Electronics Department, University of Bristol, U.K. Her work is focused on highly efficient power amplifier design for wireless communications.

Ms. Wang received two Best Student Paper Awards, at 2006 IEEE MTT-S MTT-S International Microwave Symposium, San Francisco, and 2006 IEEE MTT-S Silicon Monolithic Integrated Circuits in RF Systems (SiRF), San Diego.

Srdjan Glisic received the B.S. degree in electrical engineering from the Faculty of Electronic Engineering, Nis, Serbia, in 2000. He joined the Circuit Design Department of IHP, Frankfurt (Oder), Germany, in 2003 as a Ph.D. candidate. He is involved in projects on 60 GHz wireless communication and automotive radar in 77 GHz frequency range. He works mainly on VCOs, PLLs, amplifiers as well as mixers, dividers, PAs, PCB design and system integration.

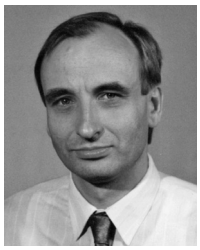

Johannes Borngraeber received the Diploma of mathematics from Humbolt University, Berlin, Germany, in 1981.

Since 1994, he has worked in the Department of Circuit Design at IHP Microelectronics GmbH. Currently he is especially interested in noise figure and phase noise measurement techniques in the millimeter-wave range.

Wolfgang Winkler received the M.S. and Ph.D. degrees, both in electrical engineering, from the Technical University Ilmenau, Germany, in 1979 and 1984, respectively.

He joined the research institute IHP in Frankfurt (Oder), Germany, in 1984 as a Design Engineer. His main research interests are circuits for wireless communication and radar in silicon-based technologies. In the last few years, he has been especially involved in the design of building blocks for wireless transceivers at 60 GHz and radar circuits at 24 and 77 GHz. Additionally, he designed benchmarking circuits for technology characterization and model verification for frequencies up to 120 GHz. He founded the company Silicon Radar in 2006. As CTO, he is now responsible for the development of SiGe-MMICs for radar and communication systems.

J. Christoph Scheytt (S'96–M'01) received the diploma degree (M.Sc.) in 1996 and the Ph.D. degree (with highest honors) in 2000, both from Ruhr-University Bochum, Germany.

In 2000, he co-founded advICo Microelectronics GmbH, a German IC design house which is dedicated to broadband and RF IC design. For six years he headed advICo and led several projects in the area of wireless and fiber-optic IC design. Since 2006, he has been with IHP where he is head of the Circuit Design Department. He has authored or coauthored around 30 papers and holds eight patents. His research interests include millimeter-wave and broadband IC design for wireless and wired communications as well as PLL techniques.